GA–A23547

# RECENT FINDINGS RELATIVE TO ADVANCED TOKAMAK MODES AND THEIR IMPLICATIONS FOR FUSION ENERGY

by
P.I. PETERSEN and The DIII–D TEAM

OCTOBER 2000

## DISCLAIMER

GA–A23547

# RECENT FINDINGS RELATIVE TO ADVANCED TOKAMAK MODES AND THEIR IMPLICATIONS FOR FUSION ENERGY

by
P.I. PETERSEN and The DIII–D TEAM

**This is a preprint of an invited paper to be presented at the 14th Topical Meeting on Technology of Fusion Energy, October 15–19, 2000, in Park City, Utah, and to be published in the *Fusion Technology.***

**Work supported by
the U.S. Department of Energy
under Contract No. DE-AC03-99ER54463**

**GA PROJECT 30033
OCTOBER 2000**

# RECENT FINDINGS RELATIVE TO ADVANCED TOKAMAK MODES AND THEIR IMPLICATIONS FOR FUSION ENERGY

P.I. Petersen and the DIII-D Team
[1]General Atomics, P.O. Box 85608, San Diego, CA 92186

## ABSTRACT

An advanced tokamak is characterized by increased confinement, stability and steady state operation. The increased confinement and stability are obtained through modifications to the shape and profiles of the plasma and through stability feedback control. These modifications have to be self-consistent. The increased confinement makes it possible to make smaller and thereby lower cost reactors for the same power output as compared to conventional tokamaks. Four potential modes for advanced tokamaks are currently being studied on DIII-D: radiative improved mode, high internal inductance $\ell_i$ mode, negative central shear (NCS) mode, and quiescent double barrier (QDB) mode.

Computer simulations have been made of the NCS modes and they show encouraging possibilities. These modes are now lasting over 2 seconds (16 $\tau_E$) in DIII-D and better understanding and off-axis current profile control (electron cyclotron current drive) are intended to extend the duration of these modes to near steady state. Six 1 MW gyrotrons have been commissioned and four have been used in the advanced tokamak experiments. Additional hardware has been and will have to be developed for the ECH system to fully utilize it: diamond windows and long-pulse launchers. Power supplies have been installed to drive an array of external saddle coils and use them to stabilize the resistive wall modes. A new upper-inner divertor has been installed in DIII-D to study the effect of closed divertor versus open divertor.

## I. INTRODUCTION

The primary focus of the advanced tokamak[1] program is to optimize the tokamak as a magnetic confinement system through control of the plasma shape, and internal profiles and active control of MHD instabilities. System studies[2,3] have shown that an optimal fusion power plant requires high energy confinement $\tau_E$ for ignition margin and compact size; high plasma pressure or beta, $\beta_T = 2\mu_0\langle P\rangle/B_T^2$ for high power density; and high bootstrap fraction for low recirculating power and steady state operation. The bootstrap current is the current which is self-driven by the plasma pressure gradient and requires no external drive. In order to control such a plasma, it has to be well diagnosed and the right tools have to be in place to control the plasma.

In the DIII-D research program three different modes that have the potential to be developed into an advanced tokamak mode have been identified and a fourth possibility has been discovered recently. The three modes are the radiative improved mode, the high $\ell_i$ mode, and the negative central shear mode (NCS). The recently discovered mode is called the quiescent double barrier mode.

The three different advanced tokamak modes will be described in Sections II through IV with a short description of the quiescent double barrier mode in Section V. Section VI will discuss high density plasmas, which are of interest for reactors. Section VII will discuss internal transport barriers, which lead to the good confinement in advanced plasmas, and Section VIII will cover resistive wall modes, which currently limit the duration of and the maximum energy obtainable in negative central shear plasma discharges. Section IX will describe divertors, which are used to control the particle flow and the heat load on the reactor floor. Section X covers the electron cyclotron heating hardware upgrades that are being implemented for the advanced tokamak experiments on the DIII-D tokamak. Finally the implications of the findings relating the advanced modes for future tokamak reactors will be discussed in Section XI.

## II. RADIATIVE IMPROVED MODE

The radiative improved mode is obtained by injecting impurity gases into the edge of the plasma, which increases the radiation in the edge. Intrinsic impurities[4] in tokamak discharges, namely carbon, oxygen, and medium or high Z metals, have generally been regarded as deleterious to sustain high performance and reproducible discharges. However, non-intrinsic impurities have been shown, under some conditions, to produce confinement improvements above L-mode[5] scaling and the radiating mantle that normally accompanies these impurities can minimize the peak heat flux to the plasma facing surfaces by spreading the power over a larger surface area.

The radiative improved mode holds the promise of a regime that can maintain high confinement at very high densities; approaching or exceeding the Greenwald[6] density limit and with the major portion of the plasma energy radiated from the plasma periphery. [The "Greenwald density limit" ($10^{20}$ $m^{-3}$) $\cong$ $I_p$ (MA)/$a^2$(m) is an empirical limit which has been found to describe the highest line-averaged density attainable in edge-fueled diverted tokamak discharges.] The first study of this mode was done on ISX-B[1] and since, extensively in TEXTOR.[2]. Both ISX-B and TEXTOR have nearly circular cross-section. Non-intrinsic impurities were also puffed into diverted tokamaks: ASDEX-U, JFT-2M, JET, and DIII-D with a improvement in confinement over the L-mode, but lower than H-mode (high confinement mode). The mechanism for the improvement has not been well understood.

In recent RI-mode plasmas, which have an internal transport barrier, the injection of neon leads to a further increase in the confinement and the stored energy. Both the ion and electron temperature profiles and the electron density profiles broaden. The far infrared scattering and the beam emission spectroscopy diagnostics show a concurrent reduction in the turbulence amplitude. The reduction in transport is a synergistic effect of reduced turbulence drive from the injection of impurities and increased E×B flow, which stabilizes microturbulence. However, the incremental confinement improvement decreases with increasing toroidal field.

## III. HIGH $\ell_I$ MODE

Both $\tau_E$ and $\beta^{max}$ have been shown to increase with increasing internal inductance $\ell_i$, which would appear to make the high $\ell_i$ scenario[9,10] very attractive scenario for advanced tokamaks performance. However, the ability to maintain high $\ell_i$, consistent with significant bootstrap current presents a challenge. High $\ell_i$ plasmas have been obtained by negative plasma current ramp or by rapidly increasing the plasma volume. These techniques are clearly transitory in nature. When the current profile becomes fully relaxed, with significant bootstrap current, $\ell_i$ becomes reduced and the confinement and stability improvements are limited, making the mode less attractive with fully-consistent steady-state profiles. However, there a number of reasons that makes it worth studying the mode further: (1) it is compatible with the RI-mode, (2) on-axis current drive is more efficient because of higher temperature and the absence of trapped particle, (3) the improvement with $\ell_i$ appears to have no threshold in input power, density etc., and (4) normalized beta ($\beta_N$ = $\beta$/(Ia/B), where I is the plasma current, a is the minor radius of the plasma, and B is the magnetic field) values up to 4 are calculated to be stable without wall stabilization. DIII-D plans to exploit the high $\ell_i$ mode in the future when higher central current drive power is available.

## IV. NEGATIVE CENTRAL SHEAR (NCS) MODE

Steady-state advanced tokamak scenarios will necessarily have a high bootstrap fraction in order to minimize the recirculating power and maximize the energy gain. Since the "natural" profile of the bootstrap current is a hollow current profile, it becomes natural to ask what is the performance potential for such profiles. The NCS regime combines high confinement, potentially high beta limits with wall stabilization, and high bootstrap fraction with the bootstrap current well-aligned with the required current profile.[11,12]

The most often used technique to establish the required current profile and q profile is the application of auxiliary heating during the current ramp up phase. An example of a typical DIII-D discharge evolution is shown in Fig. 1,[13] comparing the q profile evolution with and without heating during the current ramp. Just following the plasma breakdown, q is everywhere very high. Auxiliary heating during the current drive phase tends to "freeze" in the current, driving the toroidal electric field near zero on axis. The applied electric field during the current ramp drives a current that has a maximum off axis.[14] The different q profiles shown are those with different levels of early beam heating. The bootstrap current, with a maximum off axis, can contribute to hollow current profile, especially in the early low current moderately high $\beta_N$ phase. With ohmic current drive only, the profile slowly diffuses to a profile peaked on axis with a monotonic q profile. The magnitude of the magnetic shear reversal can be controlled by the magnitude and timing of the auxiliary heating, the target density, and thedelay in the plasma current flattop until the time of interest, generally when additional heating is applied.

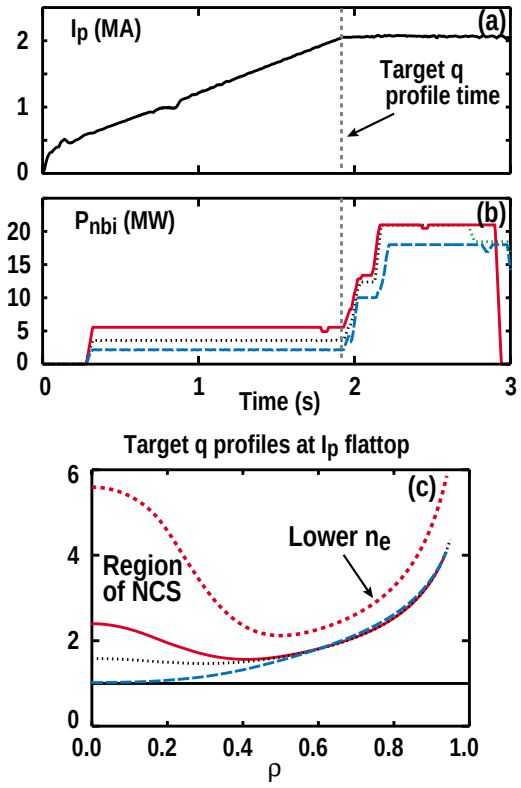


Fig. 1. NCS is reproducibly obtained with auxiliary heating during the current ramp. Shown is typical (a) plasma current (b) auxiliary heating, and (c) q-profiles.

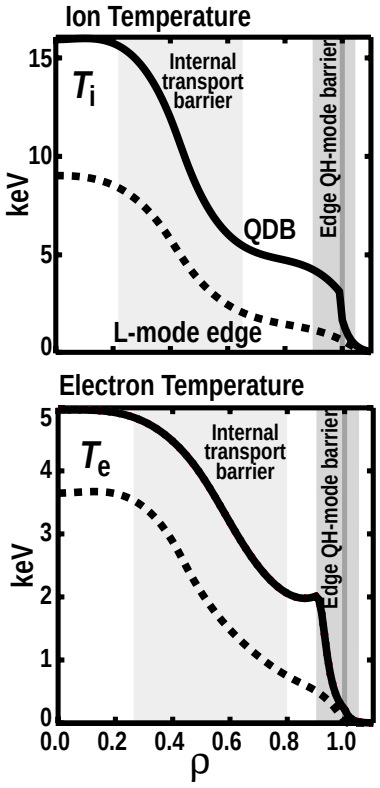


Fig. 2. Profiles of ion and electron temperatures for two plasmas with internal transport barriers: one with an L–mode (barrier-free) edge (dashed), and another in the "Quiescent Double-Barrier" mode. Note that the edge barrier adds a nearly constant pedestal onto the temperature profiles achieved with an L–mode edge. A temperature of 10 keV is 110 million degrees centigrade.

In recent experiments in DIII-D a high performance NCS ELMing H–mode was obtained with $\beta_N H_{89} \sim 9$ for 16 energy confinement times. The bootstrap fraction was 50% and and the discharge performance ($\beta$) was limited by resistive wall modes near the calculated no-wall ideal limit, which is approximately $\beta_N \sim 4\,\ell_i$

## V. QUIESCENT DOUBLE BARRIER MODES

Very recently a new mode[15] of advanced tokamak operations was discovered in DIII-D. The mode is called the quiescent double barrier mode (Fig. 2) and has both an internal and an edge transport barrier. It is obtained with counter-injection of neutral beams, which gives a broader internal transport barrier and an edge transport barrier, which raises the plasma temperature everywhere in the plasma, increasing the fusion reactivity. It has an ELM-free H-mode edge with impurity and density control so that steady-state appears possible. A continuous multi mode MHD activity inhibits ELMs. Advantages of QDB is that it has no ELMs. The absence of ELMs in the QDB is advantageous for obtaining internal transport barriers and eliminating large pulsive heat flux to the first wall. Previously large ELMs would destroy the internal transport barrier and the significant energy loss during the ELMs shows up as large short bursts of heat to the divertor and first wall. However, today QDB has only been obtained with counter neutral beam injection, and operational scenarios consistent with steady-state have not yet been identified.

## VI. HIGH DENSITY PLASMAS

Some recent experiments in DIII-D with lower single null plasmas have allowed operations at high densities up to 1.4 times the Greenwald limit with high confinement $H_{89P} \approx 1.9$ (Fig. 3). In these shots the stored energy increases monotonically during the density rise. The density rise shows no signs of saturation. The high confinement phase is terminated after the onset of 3/2 MHD mode. In these experiments the energy lost during an ELM was found to decrease by a factor of 4–5 as density increases (Fig. 4). The decrease was found to have a threshold, which is at a higher density for higher triangularity. The previous scaling[16] predicts ELMs that eject energy a factor of 3–4 too large for the ITER's

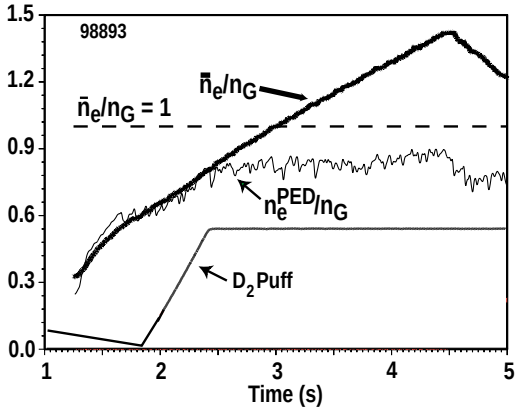


Fig. 3. The line average density rises continuously during the gas puff phase until the high confinement mode is terminated by a 3/2 MHD mode at which point it has reached ~1.4 $n_G$.

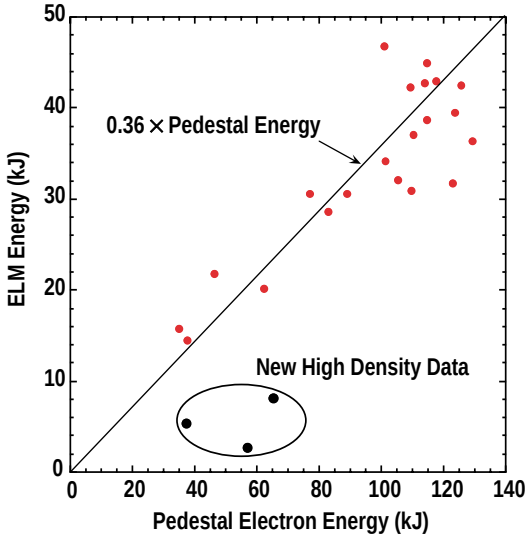


Fig. 4. At low density the ELM energy scales as about 1/3 the pedestal energy in DIII-D. At high density the ELM energy is a factor 4-5 lower.

divertor at the desired pedestal values causing excessive erosion of the divertor files. Thus the new data indicating lower energy loss during ELMs at high density is very encouraging for reactor designs.

## VII. INTERNAL TRANSPORT BARRIERS

One of the scientific successes of fusion research is the development of a model[17] to explain the formation of transport barriers in all the high perormance operation modes mentioned above. The fundamental physics involved in the transport reduction is the effect of E×B velocity shear on the growth and radial extent of turbulent eddies in the plasma. The stabilization is due to two effects. The first is that the presence the E×B velocity shear results in enhanced damping by coupling the unstable modes to other, nearby, more stable modes. The second is reduction in radial transport owing to a decrease in the radial correlation length and the change in the phase between density, temperature, and potential fluctuations. The reason that the velocity shear plays a role in so many different situations is that there are a number of ways to establish the radial electric field $E_r$. The radial force balance equation can be written as

$$E_r = (Z_i e n_i)^{-1} \nabla P_i - v_{\theta i} B_\phi + v_{\phi i} B_q \quad , \qquad (1)$$

where $Z_i$, is the ion charge number, e the electron charge, $n_i$ is the ion density, and $\nabla P_i$ is the gradient of the pressure; $v_{\phi i}$ and $v_{\theta i}$ are the toroidal and poloidal fluid velocities, and $B_\phi$ and $B_\theta$ are the toroidal and the poloidal magnetic fields. Thus, the radial electric field can be created by the pressure gradient, the poloidal flow and/or the toroidal flow. In DIII-D, where the neutral beams are injected in the direction of the plasma current, $v_\phi B_\theta$ is the major contributor to the radial electric field. Figure 5 shows a comparison of L-mode and H-mode discharges near the time of an L to H transition in a double-null 1.5 MA plasma. The toroidal field is 2.2 T, and 8.6 MW of deuterium neutral beam power is injected into the plasma, which has a line average density of $3.6\times10^{19}$ $m^{-3}$. The L-mode time is 50 ms prior to the start of the dithering transition, while the H-mode is 50 ms later in the quiescent H-mode phase. In the L-mode, the radial electric field $E_r$ changes gently from the center to the edge, and the E×B velocity shear rate $\omega_{E\times B}$ is comparable to the nonlinear turbulence decorrelation rate $\Delta\omega_D$ in the whole plasma. The vertical bar indicates the uncertainty in $\omega_{E\times B}$. For the H-mode, there is a characteristic well in $E_r$ near the edge and a large gradient. The E×B velocity shear $\omega_{E\times B}$ is much greater than $\Delta\omega_D$ near the edge, and gives rise to an ion transport barrier there.

Performance of NCS discharges with internal transport barrier and peaked pressure profiles is limited by disruptions near the calculated beta limit. Calculations[18,19] show that a broadening of the pressure profile can increase the stability limit. In DIII-D, the pressure profile can be broadened transiently by a controlled transition to H-mode during the NCS discharge. In the NCS discharge, it has been possible to extend the transport barrier and obtain ion heat transport in the neoclassical regime in the whole plasma. Using counter-injected neutral beams as shown in Fig. 6 can also broaden the ITB. In the co-injection mode, the main ion rotation and the pressure gradient components in Eq. (1). are opposing each other, whereas in the counter-injection mode they add up and thereby move the ITB further out.

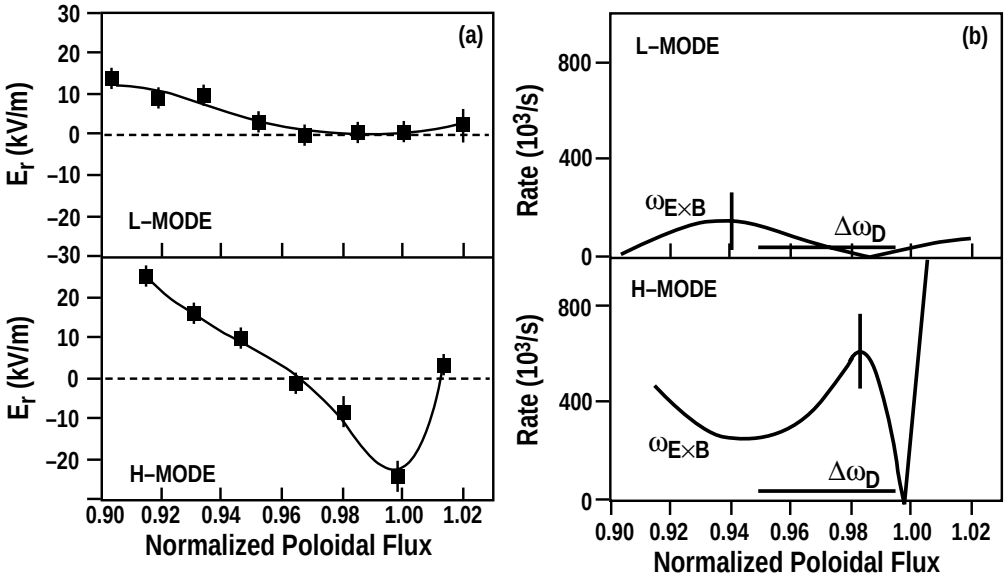


Fig . 5. Comparison of L-mode and H-mode edge profiles in DIII-D. In (a) the Er profiles are shown; notice the characteristic Er well at the plasma edge in H-mode. In (b) the ExB shearing rate $\omega_{ExB}$ is compared to the intrinsic turbulence decorelation rate $\Delta\omega_D$. In H-mode the ExB shearing rate is greater than the turbulence decorelation rate especially near the edge.

## VIII. RESISTIVE WALL MODES

Resistive wall modes[20] (RWM) are one of the primary instabilities limiting the performance of high bootstrap fraction negative central shear plasmas. The RWM seen in the DIII-D tokamak originates from an n=1 ideal external kink mode, which in the presence of a resistive wall is converted to a slowly growing RWM. The RWM is driven by the phase difference between the plasma surface perturbation and the dissipation of inductively coupled currents in the vessel wall. The characteristic time for the mode growth and rotation is the skin time of the vessel wall, which in DIII-D are a few milliseconds. This is low enough that an active feedback system[21] should be able to interact with the mode and stabilize it.

A set of sensor coils (Fig. 7) has been installed outside the vacuum vessel of DIII-D to detect the slowly varying magnetic field from the RWM, which is on the order of a few gauss to tens of gauss. The field error correction coils (C-coils) that were mounted several years ago to correct for the inherent error field[22] have been used in experiments to actively control the resistive wall mode. These coils consist of six saddle coils, each 1.6 m high, 60° wide toroidally. Each coil consists of four turns of 750MCM cable capable of carrying pulses of 5 kA for several seconds and producing a radial field up to 30 gauss at the plasma edge. Diametrically opposed coils are wired in anitseries to produce the primary n=1 field that matches most of the plasma instabilities including the RWM. The feedback control is done with the DIII-D Plasma Control System, where a dedicated fast CPU is used to perform the required fast calculations required for the RWM stabilization.

In early experiments without feedback, it was found that plasma rotation was insufficient for complete RWM suppression and that the RWM limits $\beta_N$ to the value for the no-wall case. With the active feedback it has been possible to suppress the RWM for 20 wall skin times. With additional internal sensors and 6 additional coils added to the C-Coil above and 6 below the current set of 6 coils, calculations show that it should be possible to obtain $\beta_N$ values up to 4.7, very close to the ideal wall limit of 5.

## IX. DIVERTOR

The divertor is the area in a toroidal fusion device where the charged particles transition from closed flux surfaces across the separatrix onto open field lines and the open field lines direct the plasma flow to “divertor” chamber, specifically designed to handle the heat and particle flux (Fig. 8). Two divertors are installed in DIII-D with cryo pumps to pump out the neutral particles. The divertor and its pump are used to control the density and the power flowing to the wall. By puffing impurity gasses into the divertor region the power flowing to the wall can be spread by radiation over a larger areas. The impurity injection has to be done without having too much of the impurity gas flowing into the center of the plasma and radiate the energy from that region. The lower divertor in DIII-D is called an open divertor since the area where the

particles strike the wall is open. Initially, the upper divertor (RDP1999) in DIII-D consisted of only the outer baffle and pump. In year 2000 the private flux region dome and inner cryopump and baffle plate was installed to make a more closed divertor (RDP2000). The different divertor configurations are shown in Fig. 8, which also shows that the more closed the divertor is, the better the plasma density is controlled.

Improved density and impurity control was obtained with the more closed divertor RDP2000, as shown in Fig. 8. The improved density control and precise shape and beta control using the DIII–D digital control system, were instrumental in obtaining the very long duration high-performance discharge shown in Fig. 9. The high performance ($\beta_N H_{89P} \sim 7$) was sustained for 35 energy confinement times with feedback control of $\beta$ at 95% of the stability boundary and density control at $n_e/n_G \sim 0.3$. When $\beta_N$ is increased by about 5% a 2/1 mode grows and reduces $\beta_N$ (Fig. 9).

## X. ELECTRON CYCLOTRON SYSTEM

Electron cyclotron (EC) power has proven capabilities for both heating and current drive in energetic plasmas, and is an important tool for current profile modifications and maintenance in advanced tokamaks. A series of high performance plasmas in DIII-D have a bootstrap fraction of over 50%. 75% of the current is driven non-inductively driven and the remaining 25% ohmically driven current, which is peaked at the half radius, is planned to be replaced with electron cyclotron current drive. The DIII–D EC system (Fig. 10) is being upgraded with three 1 MW sources added to the existing systems for a total power generating capacity of ~5 MW. This upgrade is based on the use of the single disc chemical vapor deposition (CVD) diamond window, 1 MW diode gyrotron, recently developed by CPI. All gyrotrons are connected to the tokamak via a low-loss, windowless, evacuated transmission line system, using circular corrugated waveguide with a 31.75 mm diameter for propagation in the $HE_{11}$ mode. Each waveguide system incorporates an in-vessel two-mirror launcher. The newest launcher can steer the rf beam poloidally from the center to the outer edge of the plasma and toroidally for either co- or counter-current drive.

At the tokamak end of the transmission system are four dual launchers (presently three are installed, a fourth dual launcher will be installed in the Summer of 2001). Each launcher is comprised of a pair of focusing mirrors and flat tilting mirrors used to steer the beam. All three installed launchers have the ability to change poloidal launch direction between successive plasma shots to change the radial location of the absorption. One has the additional capability of between shot toroidal steering which is to change the direction of the driven current (from co to radial, with no current drive, to counter). The fourth launcher will also have both toroidal and poloidal steering capability. At present, the launchers have mirrors capable of supporting pulses up to 5 s in duration. A new mirror design is currently being implemented which should support the full pulse 10 s capability of the CPI production gyrotrons.

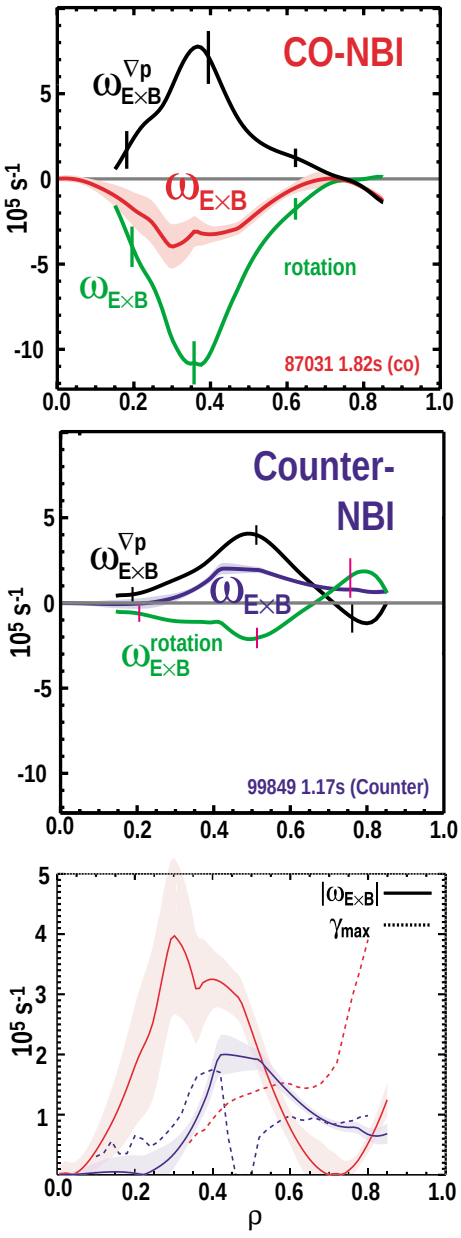


Fig. 6. In the co-injection mode, the main ion rotation and the pressure gradient components in Eq (1). are opposing each other, whereas in the counter-injection mode they add up and thereby move the ITB further out.

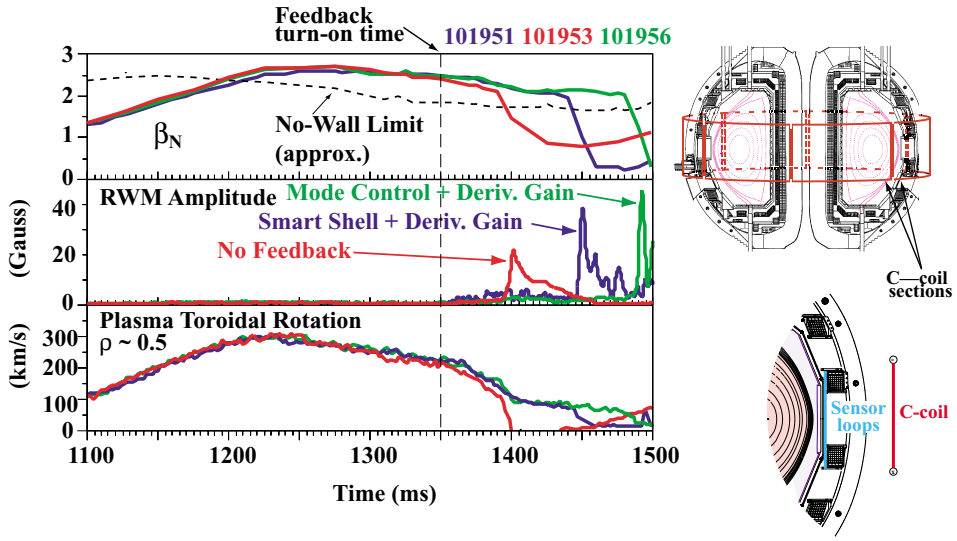


Fig. 7. With feedback control discharges with resistive wall modes have extended for more than 20 $\tau_w$ . The layout of the sensor coils and C-coils are shown in the right hand side of the drawing.

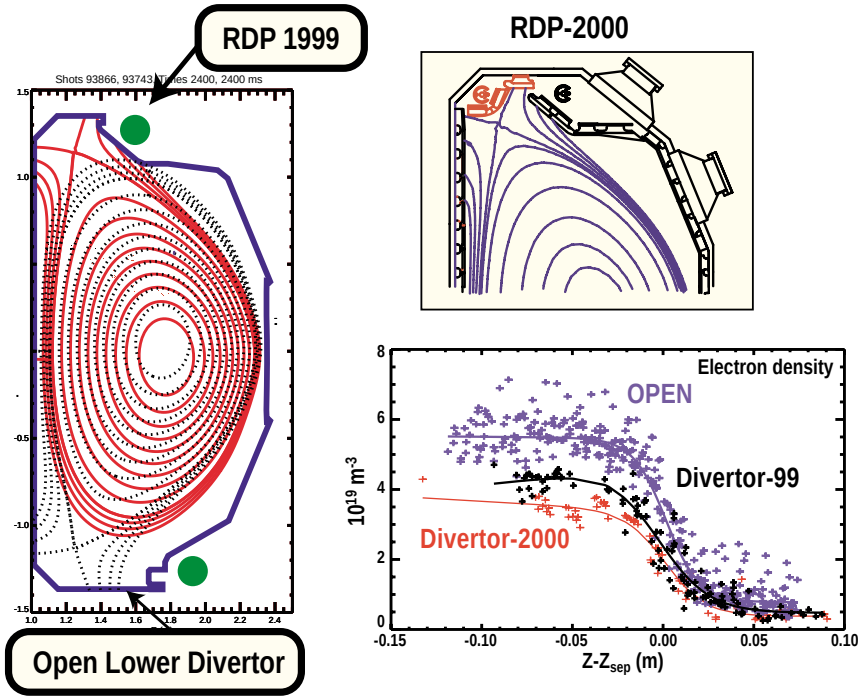


Fig. 8. A comparison between the open, RDP1999, and RDP2000 shows that the fewer neutrals and impurities, measured by the electron density, migrates into the center of the plasma, the more closed the divertor is.

In experiments performed this year, it has been possible to completely suppress the neoclassical tearing mode by localized electron cyclotron current drive in ELMing H-modes. This is a significant step toward to being able to control some plasma instability by using electron cyclotron current drive at definite positions and in very localized areas.

## XI. IMPLICATIONS FOR FUSION REACTORS

Fusion power plant design studies indicate that both high confinement and high beta are needed for attractive compact designs. High confinement is wanted to reduce the size of the device and the cost, and high beta is needed for high power density and steady state operation,

requiring a large fraction of the plasma current to be driven by bootstrap current. High beta in turn requires strong plasma shaping with high triangularity and active control of the profiles and the instabilities. $\beta_N$ of 3.5 is used in the design of JT60-SC without wall stabilization; however, profile control and some stability control will probably be required. In devices with higher $\beta_N$, wall stabilization will be required. The wall stabilization coils may need to be located inside the toroidal field coils to minimize excessive eddy current and heat load in superconducting toroidal coils.

The very limited penetration of the blanket required for electron cyclotron waves and the capability to locate the sources far away from the nuclear environment, make electron cyclotron very attractive for plasma heating, localized current profile control, and stabilization of internal MHD instabilities. Electron cyclotron waves can be delivered through fairly small (~2 in.) waveguides that do not require a straight line of sight, and thus the neutron leakage can be reduced. A similar reason makes the electron cyclotron emission diagnostic attractive.

Advanced plasma control is required for high-performance, steady-state advanced tokamak operation. Very precise control of the divertor shape is needed for heat and particle exhaust control in the divertor. Very precise deposition of the ECCD in the center of the island is required for neoclassical tearing mode stabilization. Accurate profile control is needed to maintain high performance and operate close to stability boundaries. These different control requirements (with different time constants) will necessitate an optimized multiple input, multiple output (MIMO) controller. Progress in this direction has been demonstrated with the DIII–D digital control system which is routinely used for accurate control of many plasma parameters simultaneously.

Recent experiments have shown that plasma disruption can be avoided by operating in a very controlled fashion close to the stability limit (Fig. 9). A consequence of the fact that an advanced tokamak has a lower plasma current than a conventional tokamak with the same energy confinement is that it should be easier to mitigate the effect of disruptions should they occur.

## ACKNOWLEDGMENTS

This work was performed under U.S. Department of Energy Contract No. DE-AC03-99ER54463. The author wants to thank T.S. Taylor for valuable discussions on the subject of implications of recent data on advanced tokamaks.

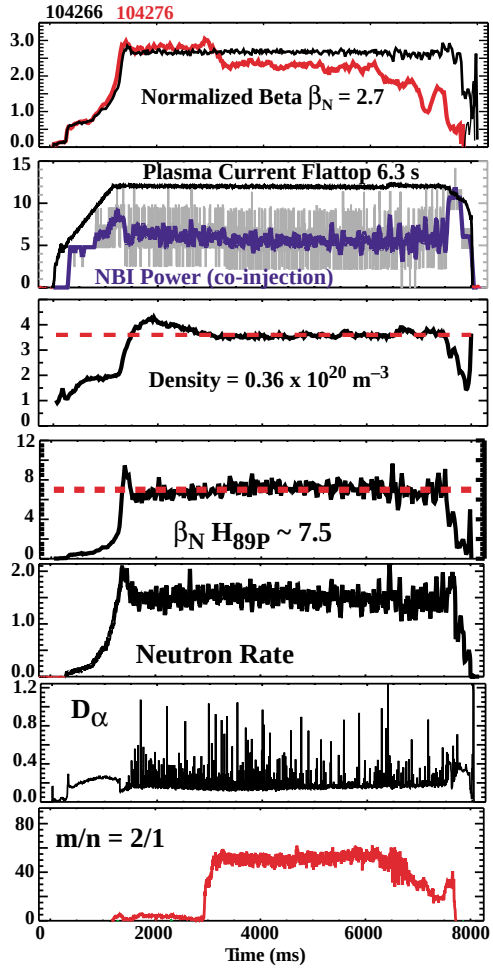


Fig. 9. The high performance ($\beta_N H_{89P}$ ~ 7) long duration discharge sustained with feedback control of $\beta$ at 95% of the stability boundary and density control with the RDP2000 divertor. When $\beta_N$ is increased a 2/1 mode grows and reduces $\beta_N$.

## REFERENCES

[1]T.S. Taylor, "Physics of Advanced Tokamaks," Proc. 24th European Conf. on Controlled Fusion and Plasma Physics, Berchtesgaden, Germany, 1997.
[2]T.S. Taylor, Plasma Phys. Control. Fusion **39** , B47 (1997).
[3]J.D. Galambos, et al., Nucl. Fusion **35**, 551 (1995).
[4]G.L. Jackson, "Effects of impurity seeding in DIII-D radiating mantle discharges," submitted to Nucl. Fusion.
[5]P.N. Rushmanov, et al., Nucl. Fusion **30**, 1999 (1990).
[6]M. Greenwald, et al., Nucl. Fusion **28**, 2199 (1988).
[7]E.A. Lazarus, et al.., Nucl. Fusion **25**, 135 (1985).
[8]B. Unterberg, et al., J. Nucl. Mater. **266–299**, 75 (1999).
[9]M. Zarnstorf, Plasma Phys. Contr. Nucl. Fusion Research 1992, Wurzburg, Austria, Vol. 1 (IAEA, Vienna, 1993) p. 111.

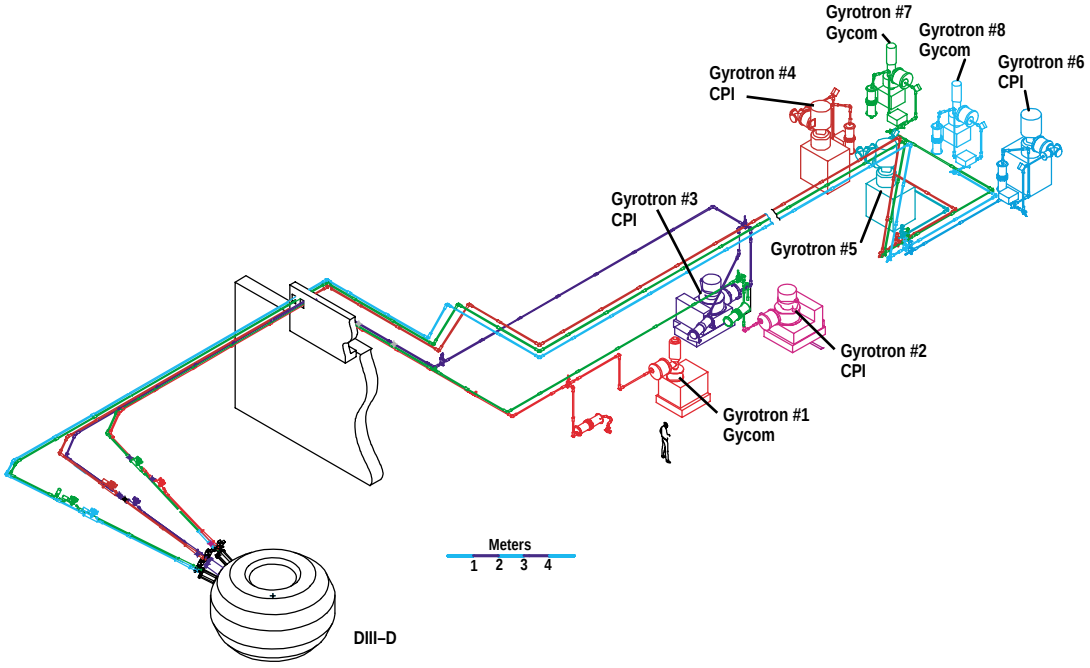


Fig. 10. Layout of the ECH system.

[10]J.R. Ferron, et al., Phys Fluids B **5**, 2532 (1993).
[11]A.D. Turnbull, et al., Phys. Rev. Lett. **74**, 718 (1995).
[12]C. Kessel, Phys. Rev. Lett. **72**, 1212 (1994).
[13]B.W. Rice, Plasma Phys. Contr. Fusion **38**, 869 (1996).
[14]B.W. Rice, et al., Plasma Phys. Contr. Fusion **38**, 869 (1996).
[15]K.H. Burrell, "Constant Density, ELM-Free, Steady-State Divertor Plasmas in DIII–D," Proc. of 42nd Ann. Mtg Division of Plasma Physics, Quebec City, Canada, 2000, to be published in Phys. Plasmas.
[16]A.W. Leonard, et al., J. Nucl. Mater. **266-269**, 109 (1999).
[17]A.D. Turnbull, et al., Plasma Phys. Contr. Nucl. Fusion Research 1996, Montreal, Canada, (Internation Atomic Energy Agency, Vienna)
[18]A.D. Turnbull, et al., "Synergism Between Cross-Section and Profile Shaping in Beta Optimization of Tokamak Equilibria with Negative Central Shear," Nucl. Fusion **38**, 1469 (1998).
[19]E.J. Strait, Phys. Rev. Lett **74**, 2483 (1995).
[20]A.M. Garofalo, et al., Phys. Rev. Lett. **82**, 3811 (1999).
[21]J.T. Scoville, et al., Proc. 18th IEEE/NPSS Symposium on Fusion Engineering, Albuquerque, New Mexico, 1999 (IEEE, New York) to be published.
[22]R.J. La Haye, et al., Rev. Sci. Instrum. **62**, 2146 (1991).

## DIII–D TEAM

S.L. Allen,[a] P.M. Anderson,[b] M.E. Austin,[c] D.S. Baggest,[b] W. Baity,[d] D.R. Baker,[b] D.E. Baldwin,[b] G. Barber,[d] R. Bastasz,[e] C.B. Baxi,[b] L. Baylor,[d] S. Bernabei,[f] J. Bialek,[g] J.A. Boedo,[h] I.N. Bogatu,[i] A. Bondeson,[j] A.S. Bozek,[b] R. Bravenec,[c] B.D. Bray,[b] D. Brennan,[k] J.D. Broesch,[b] N.H. Brooks,[b] K.H. Burrell,[b] J. Burrus,[b] J. Callen,[l] R.W. Callis,[b] T.N. Carlstrom,[b] E. Carolipio,[m] B. Carreras,[d] W.P. Cary,[b] T.A. Casper,[a] V.S. Chan,[b] M. Chance,[f] J. Candy,[b] L. Chen,[n] E. Chin,[b] H.K. Chiu,[b] S.C. Chiu,[b] M. Chu,[b] R.J. Colchin,[d] S. Combs,[d] K. Comer,[l] W. Davis,[f] J.C. DeBoo,[b] J.S. deGrassie,[b] S. Delaware,[b] R. Deranian,[o] J.L. Doane,[b] E.J. Doyle,[p] D. Edgell,[i] R. Ellis,[q] R. Ellis III,[f] D. Ernst,[f] T.E. Evans,[b] R. Feder,[f] M.E. Fenstermacher,[a] C. Fenzi,[l] J.R. Ferron,[b] D. Finkenthal,[r] R. Fonck,[l] E. Fredrickson,[f] J. Freeman,[b] M. Friend,[b] C. Fuchs,[s] S. Galkin,[t] A. Garofalo,[g] G. Garstka,[q] G. Giruzzi,[u] P. Gohil,[b] A.A. Gootgeld,[b] I. Gorelov,[b] F. Grantham,[b] D. Gray,[h] M. Gryaznevich,[v] J.M. Greene,[b] K.L. Greene,[b] C.M. Greenfield,[b] N. Greenough,[f] R.J. Groebner,[b] S. Guenter,[s] T.S. Hahm,[f] M.J. Hansink,[b] T.E. Harris,[b] R.W. Harvey,[w] T. Hatae,[x] C. Hegna,[l] W.W. Heidbrink,[m] F.L. Hinton,[b] J. Hogan,[d] E. Hollman,[h] K.L. Holtrop,[b] R.-M. Hong,[b] J. Hosea,[f] W. Houlberg,[d] C.L. Hsieh,[b] D.A. Humphreys,[b] A.W. Hyatt,[b] H. Ikezi,[b] A. Isayama,[x] R.C. Isler,[d] G.L. Jackson,[b] N. Jaluka,[y] J. Jayakumar,[a] T.H. Jensen,[b] T. Jernigan,[d] R.D. Johnson,[b] L. Johnson,[f] D.H. Kaplan,[b] K.M. Keith,[b] A.G. Kellman,[b] D.H. Kellman,[b] R. Khayrutdinov,[z] J.S. Kim,[i] J.F. Kinsey,[aa] R.J. La Haye,[b] G. Labik,[f] L.L. Lao,[b] C.J. Lasnier,[a] J. Latchem,[b] E.A. Lazarus,[d] R.L. Lee,[b] R.A. Legg,[b] A.W. Leonard,[b] J.A. Leuer,[b] Y.R. Lin-Liu,[b] L. Lodestro,[a] J.M. Lohr,[b] T.C. Luce,[b] S. Luckhardt,[h] V. Lukash,[z] J.L. Luxon,[b] M.A. Mahdavi,[b] R. Maingi,[d] C.C. Makariou,[b] M.A. Makowski,[a] . Mandrekas,[bb] J. Manickam,[f] B.B. McHarg Jr.,[b] G.E. McKee,[l] A. M. Messiaen,[cc] W.H. Meyer,[a] K.R. Middaugh,[b] R.L. Miller,[b] P.K. Mioduszewski,[d] J. Moller,[a] R.A. Moyer,[h] M. Murakami,[d] A. Nagy,[f] G.A. Navratil,[g] A. Nerem,[b] W. Nevins,[a] Y. Nikolski,[b] D.E. Nilson,[a] M. Okabayashi,[f] Y. Omelchenko,[b] R.C. O'Neill,[b] J. Ongena,[cc] T.H. Osborne,[b] L. Owens,[d] P.B. Parks,[b] A.W. Peebles,[p] B.G. Penaflor,[b] Q. Peng,[b] F.W. Perkins,[f] P.I. Petersen,[b] T.W. Petrie,[b] C.C. Petty,[b] J.C. Phillips,[b] D.A. Piglowski,[b] R.I. Pinsker,[b] P.A. Politzer,[b] D. Ponce,[b] M. Porkolab,[dd] G.D. Porter,[a] R. Prater,[b] S.G. Pronko,[b] A. Punjabi,[y] S. Raftopoulos,[f] A. Ramsey,[f] E.E. Reis, Jr.,[b] D.E. Remsen,[b] M.E. Rensink,[a] C.L. Rettig,[p] T.H. Rhodes,[p] B.W. Rice,[a] J.I. Robinson,[b] G. Rolens,[b] M. Rosenbluth,[b] D. Ross,[c] C. Rost,[dd] D. Rudakov,[h] N. Sauthoff,[f] R.I. Savercool,[b] J.M. Schachter,[b] M.J. Schaffer,[b] D.P. Schissel,[b] G. Schmidt,[f] J.T. Scoville,[b] T.C. Simonen,[b] S.M. Skinner,[b] R.T. Snider,[b] P.B. Snyder,[b] H.E. St John,[b] W. Stacey,[bb] G.M. Staebler,[b] B.W. Stallard,[a] R.D. Stambaugh,[b] P.G. Stangeby,[ee] E.J. Strait,[b] E. Synakowski,[f] H. Takahasi,[f] H. Takenaga,[x] P.L Taylor,[b] T.S. Taylor,[b] T. Terpstra,[f] D.M. Thomas,[b] S. Turgarinov,[z] A.D. Turnbull,[b] B. Unterberg,[ff] R. Vernon,[l] S. VonGoeler,[f] M.R. Wade,[d] F. Waelbroeck,[c] M.I. Walker,[b] R.E. Waltz,[b] W.R. Wampler,[e] J.G. Watkins,[e] G. Watson,[k] J.C. Wesley,[b] W.P. West,[b] J. Whaley, Jr.,[e] D.G. Whyte,[h] H. Wilson,[v] N. Wolf,[a] C.P.C. Wong,[b] K. Wong,[f] S.K. Wong,[b] F. Yin,[n] B. Zaniol,[gg] L. Zeng,[h] M. Zerbini,[ee] C. Zhang[n]

[a] Lawrence Livermore National Laboratory, Livermore, CA.
[b] General Atomics, San Diego, CA.
[c] University of Texas at Austin, Austin, TX.
[d] Oak Ridge National Laboratory, Oak Ridge, TN.
[e] Sandia National Laboratories, Livermore, CA.
[f] Princeton Plasma Physics Laboratory, Princeton, NJ.
[g] Columbia University, New York, NY.
[h] University of California, San Diego, CA.
[i] FARTECH, San Diego, CA.
[j] Chalmers University, Götteborg, Sweden.
[k] ORISE, Oak Ridge, TN.
[l] University of Wisconsin, Madison, WI.
[m] University of California, Irvine, CA.
[n] ASIPP, Hefei, Peoples Republic of China.
[o] University of Wales.
[p] University of California, Los Angeles, CA.
[q] University of Maryland, College Park, MD.
[r] Palomar College, San Marcos, CA.
[s] IPP, Garching, Germany.
[t] Keldysh Institute, Moscow, Russia
[u] Assoc.-EURATOM-CEA, Cadarache, France.
[v] UKAEA-Culham, Abingdon, UK.
[w] Comp-X, Del Mar, CA
[x] Japan Atomic Energy Research Insitute, Naka, Japan
[y] Hampton University, Hampton, VA.
[z] TRINITI, Troitsk, Russia.
[aa] Lehigh University, Bethlehem, PA
[bb] Georgia Tech, Atlanta, GA
[cc] Assoc-EURATOM-Ecoloe Royole Militaire Academy, Brussels, Belgium
[dd] MIT, Cambridge, MA.
[ee] University of Toronto, Toronto, Canada
[ff] Assoc.-EURATOM, Kernsforschunganlage, Jülich, Germany
[gg] University Pahwa, Padua, Italy.